OPEN ACCESS
CellPress

Cell Reports
Article

Signal Integration and Transcriptional Regulation of the Inflammatory Response Mediated by the GM-/M-CSF Signaling Axis in Human Monocytes

Ramon M. Rodriguez,[1] Beatriz Suarez-Alvarez,[1] Jose L. Lavín,[2] Alex M. Ascensión,[3] Monika Gonzalez,[4] Juan J. Lozano,[5] Aroa B. Raneros,[1] Paula D. Bulnes,[1] Jose R. Vidal-Castiñeira,[1] Covadonga Huidobro,[6,7] Cristina Martin-Martin,[1] Ana B. Sanz,[8] Marta Ruiz-Ortega,[9] Amaya Puig-Kröger,[10] Angel L. Corbí,[11] Marcos J. Araúzo-Bravo,[3,12] Ana M. Aransay,[4,13] and Carlos Lopez-Larrea[1,14,15,*]

[1]Translation Immunology Laboratory, Instituto de Investigación Sanitaria del Principado de Asturias-ISPA, Oviedo, Spain
[2]Bioinformatics Unit, CIC bioGUNE, 48160 Derio, Bizkaia, Spain
[3]Computational Biology and Systems Biomedicine Research Group, Biodonostia Health Research Institute, 20014 San Sebastián, Spain
[4]CIC bioGUNE, 48160 Derio, Bizkaia, Spain
[5]CIBERehd, Plataforma de Bioinformática, Centro de Investigación Biomédica en Red de Enfermedades Hepáticas y Digestivas, Barcelona, Spain
[6]Instituto de Investigación Sanitaria del Principado de Asturias, 33011 Oviedo, Spain
[7]Centro de Investigación Biomédica en Red-Enfermedades Respiratorias (CIBERES), Instituto de Salud Carlos III, Madrid, Spain
[8]Nephrology, IIS-Fundación Jiménez Díaz, Universidad Autónoma Madrid (UAM), 28040 Madrid, Spain
[9]Cellular Biology in Renal Diseases Laboratory, Universidad Autónoma Madrid, IIS-Fundación Jiménez Díaz, Madrid, Spain
[10]Laboratorio de Inmuno-Metabolismo, Hospital General Universitario Gregorio Marañón, Instituto de Investigación Sanitaria Gregorio Marañón, Madrid, Spain
[11]Centro de Investigaciones Biológicas, Consejo Superior de Investigaciones Científicas (CSIC), Madrid, Spain
[12]IKERBASQUE, Basque Foundation for Science, 48013 Bilbao, Spain
[13]CIBERehd, ISCIII, Madrid, Spain
[14]Department of Immunology, Hospital Universitario Central de Asturias, Oviedo, Spain
[15]Lead Contact
*Correspondence: inmuno@hca.es
https://doi.org/10.1016/j.celrep.2019.09.035

SUMMARY

In recent years, the macrophage colony-stimulating factor (M-CSF) and granulocyte-macrophage CSF (GM-CSF) cytokines have been identified as opposing regulators of the inflammatory program. However, the two cytokines are simultaneously present in the inflammatory milieu, and it is not clear how cells integrate these signals. In order to understand the regulatory networks associated with the GM/M-CSF signaling axis, we analyzed DNA methylation in human monocytes. Our results indicate that GM-CSF induces activation of the inflammatory program and extensive DNA methylation changes, while M-CSF-polarized cells are in a less differentiated state. This inflammatory program is mediated via JAK2 associated with the GM-CSF receptor and the downstream extracellular signal-regulated (ERK) signaling. However, PI3K signaling is associated with a negative regulatory loop of the inflammatory program and M-CSF autocrine signaling in GM-CSF-polarized monocytes. Our findings describe the regulatory networks associated with the GM/M-CSF signaling axis and how they contribute to the establishment of the inflammatory program associated with monocyte activation.

INTRODUCTION

Monocytes are short-lived blood mononuclear cells of myeloid origin that are involved in inflammatory processes and innate immunity (Italiani and Boraschi, 2014; Wynn et al., 2013). In response to inflammation, monocytes are rapidly recruited to the injured tissue, where they are able to differentiate into macrophage-like cells, guided by the cytokine milieu and the interplay with other cells and microbial products. The combination and magnitude of the environmental cues allow monocytes to adapt to the different requirements during the inflammation process (Lawrence and Natoli, 2011; Martinez and Gordon, 2014; Sica and Mantovani, 2012). As a result, monocyte-derived macrophages can be found in different activation states, contributing to the intensification of the inflammation or to its resolution by producing anti-inflammatory cytokines and inducing tissue repair (Biswas and Mantovani, 2010; Funes et al., 2018). To develop the required level of plasticity, monocytes must be able to respond to a wide variety of pro-inflammatory and anti-inflammatory stimuli. Among these, granulocyte-macrophage colony-stimulating factor (GM-CSF) and macrophage CSF (M-CSF) have been found in recent years to be essential mediators during monocyte polarization, since they can induce many of the phenotypic features associated with pro-inflammatory and anti-inflammatory states, respectively (Lacey et al., 2012; Sander et al., 2017; Verreck et al., 2004).

The apparent antagonism between GM-CSF and M-CSF and their central role during monocyte differentiation have led to

both factors being proposed as valuable therapeutic targets. In cancer, the polarization of tumor-associated macrophages (TAMs) toward anti-inflammatory phenotypes has been linked to tumor progression, suppression of T cell function, and angiogenesis (Aras and Zaidi, 2017). GM-CSF and M-CSF signaling fulfill opposing roles during infiltration and maturation of tumor macrophages, and targeting the M-CSF receptor greatly reduces anti-inflammatory TAM infiltration in animal models and cancer patients (Neubert et al., 2018; Ries et al., 2014; Van Overmeire et al., 2016). On the other hand, GM-CSF targeting has been explored in the context of treating autoimmune diseases, giving rise to clinical trials for rheumatoid arthritis, psoriasis, and asthma (Hamilton et al., 2016; Shiomi et al., 2016). Nonetheless, since the two cytokines can be simultaneously present in the inflamed tissue, it is not clear how signaling is integrated during monocyte cell fate decisions or whether monocytes can fully reverse their phenotypes in response to apparently conflicting polarization cues.

Epigenetic mechanisms that alter gene activity without changes of the DNA sequence, such as DNA methylation or post-translational modifications of histones, are critical during cell differentiation. Recent studies have demonstrated that monocytes undergo widespread epigenetic remodeling in response to polarization signals including lipopolysaccharide (LPS), β-glucan (BG), tumor necrosis factor (TNF), and GM-CSF, suggesting that the chromatin acts as an integration node during monocyte cell fate decisions in the inflammation site (Park et al., 2017; Ramirez et al., 2017; Saeed et al., 2014). To better understand how undifferentiated monocytes integrate the GM-/M-CSF signaling axis at the chromatin level, we analyzed DNA methylation and assayed transposase-accessible chromatin using sequencing (ATAC-seq) in *ex vivo* isolated human monocytes. Our results indicate that integration of GM-CSF and M-CSF signals differs significantly, showing opposing actions that are reflected at the transcriptional and chromatin levels.

RESULTS

Transcriptional Networks during Long-Term Monocyte Polarization with M-CSF and GM-CSF

In order to study how transcriptional programs are modified during polarization, we first differentiated human monocytes over 7 days with M-CSF (Mø-M monocytes) or GM-CSF (Mø-GM monocytes). Transcriptome analysis of these cells with HumanHT-12 v4 Expression BeadChips showed extensive reprogramming in response to GM-CSF (2,501 differentially expressed genes) and M-CSF (2,339 genes) (Figure 1A), although approximately 70% of the annotated genes were shared by Mø-GM and Mø-M, indicating a close correlation between the two cell populations (Figure 1B; Table S1). Gene ontology analysis indicated that the regulated genes during monocyte polarization perform functions typically associated with monocyte/macrophages, metabolism, and apoptosis (Table S2). We observed that Mø-M preferentially overexpressed genes associated with response to wounding (*NINJ1*, *F13A1*, *SCARB1*, and *STAB1*), inflammation (*AOAH*, interleukin 10 [*IL10*], *TLR7*, *A2M*, etc.), and endocytosis (*FNBP1*, *CD209*, *SH3KBP1*, and *ITSN1*), while genes overexpressed in Mø-GM were mostly those involved in cell-cycle functions (*CCNA2*, *CDC20*, *AURKA*, *PRC1*, etc.), immune response/inflammation (*IL1B*, *CCL23*, *CXCL5*, *FCGR2B*, etc.), and glycolysis (*ALDOA*, *LDHA*, *HK2*, *PFKP*, *GAPDH*, etc.) (Table S2). Many of these functions were also highlighted within the topology of the functional interaction network derived from the genes differentially expressed between Mø-GM and Mø-M, including cell cycle, interferon response, adhesion/chemotaxis, leukotriene synthesis, glucose metabolism, and intracellular signaling (Figure 1C).

The fact that the proliferation signature was clearly overrepresented in Mø-GM raised a question about the proliferative potential of human monocytes (Figure S1A). *In vitro* polarization of human monocytes is often considered post-mitotic. However, tracking cell division by CFSE staining confirmed that, while human monocytes are not highly proliferative *in vitro*, a small percentage of cells were able to complete one replication cycle after 7 days exposure to GM-CSF or M-CSF (Figure S1B), although we observed more proliferation in Mø-GM cultures. This explains the relative overexpression of cell-cycle-related genes in these cells.

Correlation between Gene Expression and DNA Methylation Changes in Polarized Monocytes

To investigate transcription regulation during polarization, we studied this process at the epigenetic level, focusing our analysis on DNA methylation. As a reference, we included undifferentiated CD34+ cells in the DNA methylation analysis (Figure 2A). Comparison of undifferentiated CD34+ with CD14+ monocytes (Mo) confirmed that DNA demethylation was significantly more frequent (9,660 demethylated regions, $\Delta M > 1.5$ and an adjusted false discovery rate [FDR] $p < 0.05$) than *de novo* methylation (1,935) (Table S3), corroborating the demethylation trend associated with hematopoietic differentiation observed in other studies (Lee et al., 2012; Kundaje et al., 2015; Rodriguez et al., 2015). On the other hand, methylome analysis of human monocytes with GM-CSF or M-CSF showed widespread DNA methylation changes (Table S3). With this analysis we identified 2,051 differentially methylated regions (DMRs) in Mø-GM (corresponding to 1,051 genes) and only 740 (405 genes) in Mø-M (Figure 2A). In addition, most DMRs in Mø-M were included in Mø-GM (Figure 2B), suggesting that Mø-M may represent a less differentiated state. However, it should be pointed out that we annotated 219 DMRs that were specifically associated with M-CSF. In any case, GM-CSF-induced polarization was associated with much more extensive DNA methylation remodeling in which most (> 70%) of the DMRs corresponded to DNA demethylation events (Figure 2C).

DNA methylation changes annotated during monocyte polarization accumulated mostly in genes involved in immune functions associated with monocytes/macrophages (Table S4), although pro-inflammatory functions were more highly enriched in Mø-GM. Gene ontology analysis showed that many of the genes differentially methylated between Mø-GM and Mø-M were associated with signal transduction (Table S4). These results were clearly observed in the functional interaction network generated with these DMRs, in which signal transducers occupied the most central position within the network (*SRC*, *RHOG*,

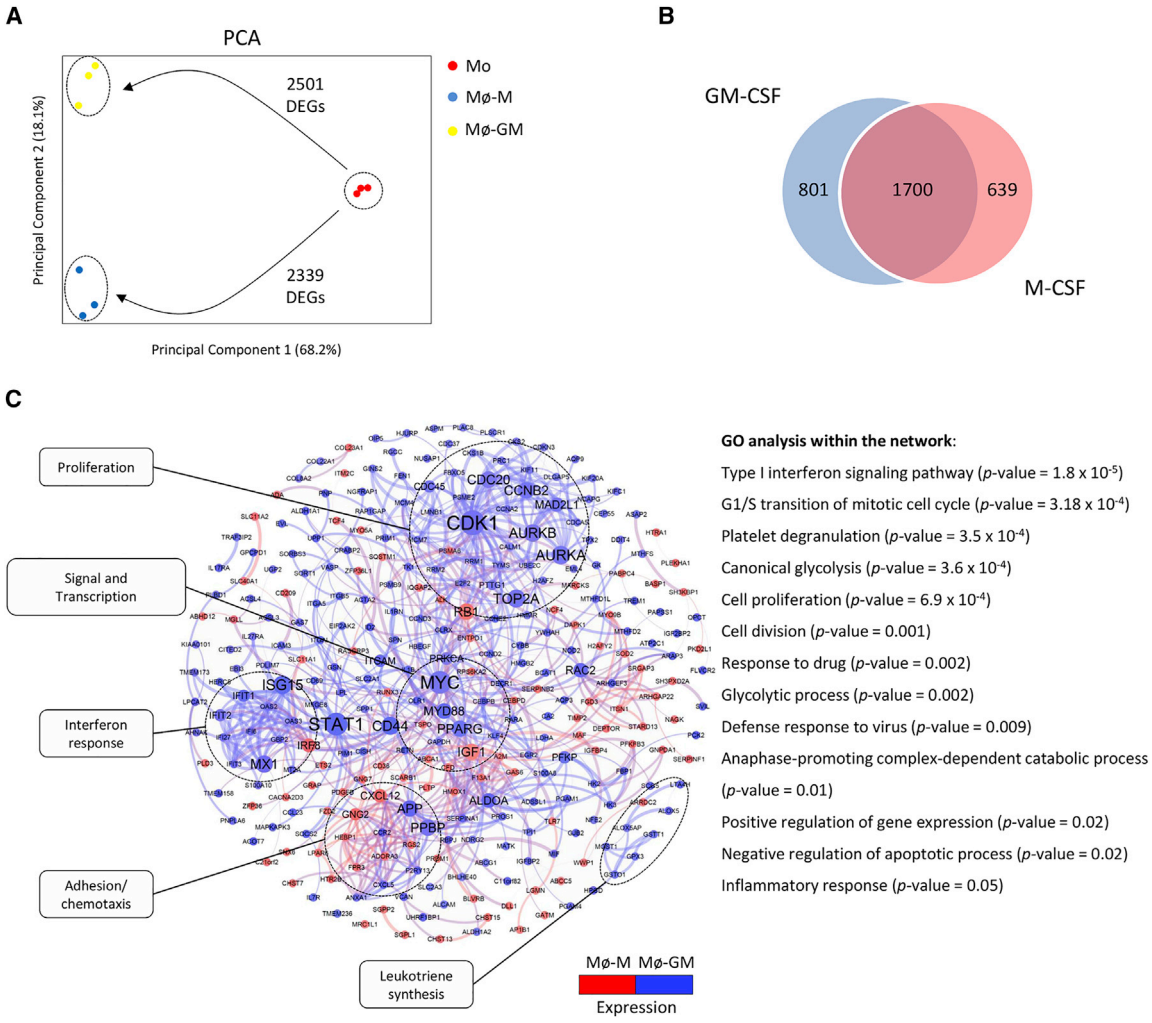

Figure 1. Gene Expression Analysis in Mø-GM and Mø-M Cells

(A) Principal component analysis of gene expression profiles (three biological replicates, each of which was obtained from a pool of three individuals).

(B) Venn diagrams showing the number of genes differentially expressed during polarization with GM-CSF and M-CSF.

(C) Functional interaction networks of genes differentially expressed between Mø-GM and Mø-M cells. Mø-GM-upregulated genes are highlighted in blue; Mø-M in red. Node size represents centrality (number of edges) in the network. Gene Ontology analysis includes only genes differentially expressed within the network. Major functions are indicated within the network topology.

and *AKT*) (Figure 2D). In addition, DNA methylation data were validated by pyrosequencing analysis of seven genes annotated as differentially methylated between Mø-GM and Mø-M in our datasets (Figure 2E).

On the other hand, the distribution of all annotated DMRs according to gene location showed that most changes accumulated in the 5′ UTR and gene body regions, but were less frequent in the first exon and between the transcription start site (TSS) and 0.2 kb (TSS200) or 1.5 kb (TSS1500) upstream of the TSS of the annotated genes (Figure 3A). Moreover, epigenetic marks often act in a coordinated manner to fine-tune chromatin function and transcription. To study how DNA methylation is associated with histone marking in activated monocytes, we compared our data with a previously published analysis of histone marking in human monocytes activated with GM-CSF (3 days) (Schmidt et al., 2016). In this study, H3K4me3 signals near TSS (±2.5 kb) and H3K4me1 signals up- or downstream of the TSS (> 2.5 kb) were used to define promoter and enhancer sites, respectively. These regulatory regions were classified according to histone occupancy in accessible promoters (H3K4me3+/H3K27Ac+), poised promoters (H3K4me3+/H3K27me3+), strong enhancers (H3K27Ac+/H3K4me1+), and poised enhancers (H3K4me1+/H3K27me3+). We observed that approximately 20% of the annotated DMRs in response to GM-CSF or M-CSF were located in accessible promoters and 12% in strong enhancers, while they were mostly absent from poised regions (< 3%) (Figure 3B). Finally, our data showed an inverse correlation between DNA methylation and expression during polarization with GM-/M-CSF in 231 genes associated with 266 CpG sites, most of which (196 genes) were demethylated and overexpressed genes

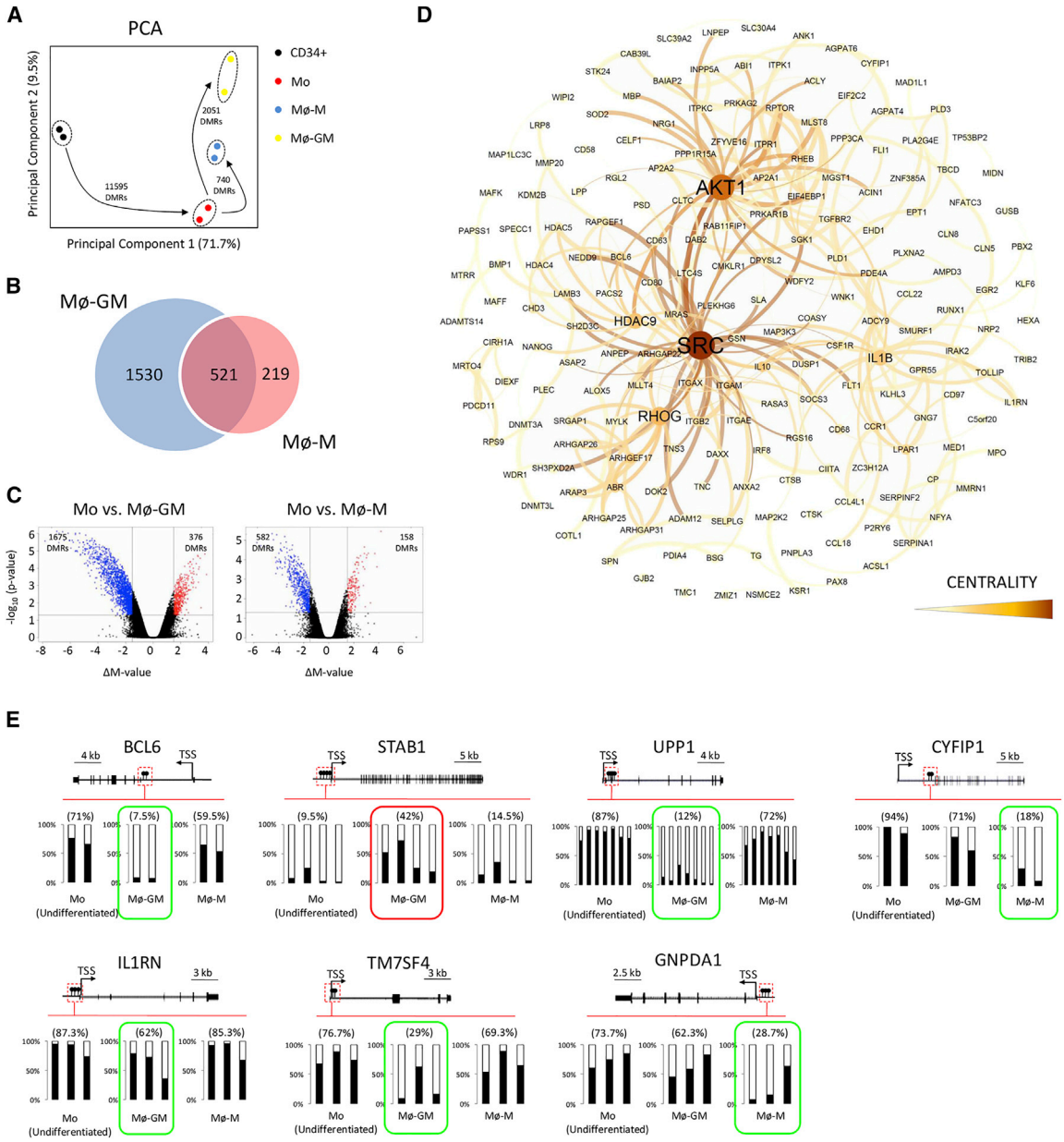

Figure 2. DNA Methylation during Long-Term Polarization with M-CSF and GM-CSF

(A) Principal component analysis of DNA methylation profiles (two biological replicates, each of which was obtained from a pool of three individuals).

(B) Venn diagrams showing the number of DMRs acquired during polarization with GM-CSF and M-CSF.

(C) Volcano plots of regions differentially methylated during polarization. Demethylated probes are shown in blue and *de novo* methylated probes are in red ($\Delta M > 1.5$, $p < 0.05$).

(D) Functional interaction networks of genes differentially methylated between Mø-GM and Mø-M cells. Network centrality is indicated by the color scale and node size.

(E) DNA methylation analysis by bisulfite pyrosequencing of selected genes differentially methylated between Mø-GM and Mø-M cells. Demethylation is indicated in green and *de novo* methylation is in red.

(Figure 3C). These DMRs are frequently located in the 5′ UTR and gene body regions (Figure 3D), but histone occupancy data showed that approximately 50% of the DMRs associated with gene expression changes overlapped with chromatin regions identified as accessible promoters (H3K4me3+/H3K27Ac+). This demonstrates that these DMRs are mostly located in regulatory regions associated with active transcription (Figure 3E).

Although M-CSF and GM-CSF are often considered to be opposite polarization signals, our DNA methylation data suggested that Mø-M cells are less differentiated than Mø-GM

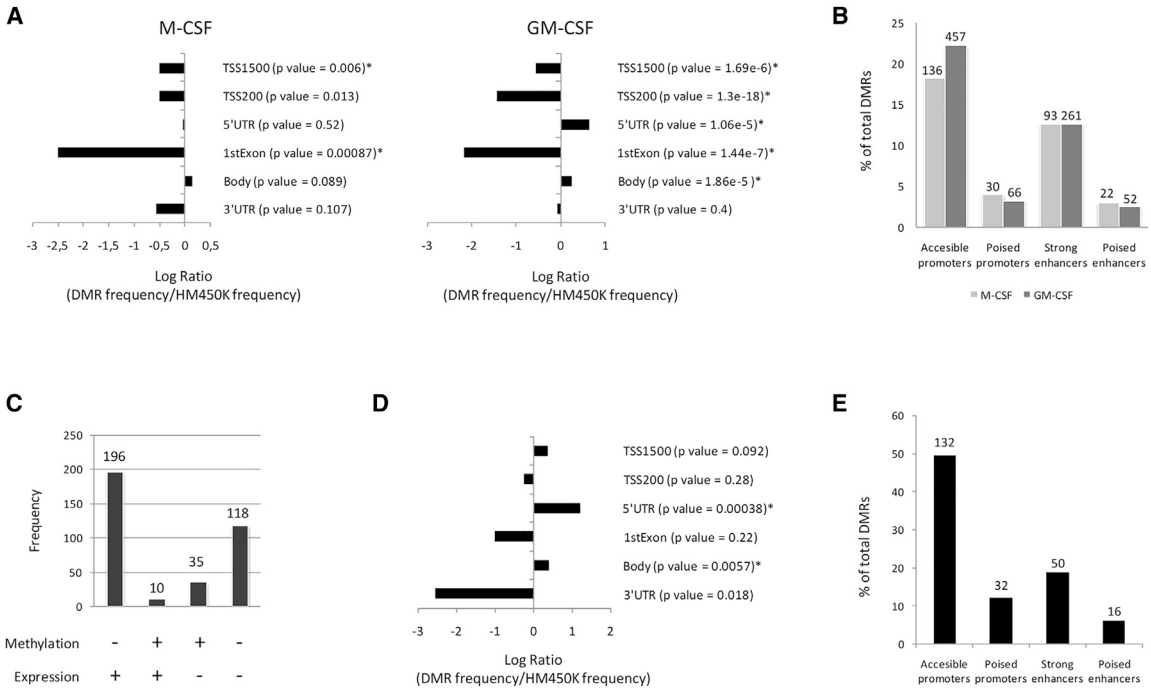

Figure 3. Genomic Distribution of DMRs during Monocyte Polarization

(A) Distribution of DMRs by gene location. Results are represented as the ratio between observed and expected frequencies. Statistical significance was evaluated by the hypergeometric test. *$p < 0.01$.

(B) DMR frequency in monocytes polarized with M-CSF or GM-CSF by histone occupancy in accessible promoters (H3K4me3+/H3K27Ac+), poised promoters (H3K4me3+/H3K27me3+), strong enhancers (H3K27Ac$^+$/H3K4me1+), and poised enhancers (H3K4me1+/H3K27me3+). The total number of DMRs is indicated on each bar.

(C) Number of differentially expressed genes (> 2-fold change, $p < 0.05$) associated with DNA methylation changes. Plus sign (+) indicates *de novo* methylation or gene-expression upregulation; minus sign (−) indicates demethylation or gene-expression downregulation. Statistical significance was evaluated by the hypergeometric test. *$p < 0.01$.

(D) Distribution of DMRs associated with gene expression changes according to gene location.

(E) Frequency of DMRs associated with gene expression changes according to histone occupancy in accessible promoters (H3K4me3+/H3K27Ac+), poised promoters (H3K4me3+/H3K27me3+), strong enhancers (H3K27Ac+/H3K4me1+), and poised enhancers (H3K4me1+/H3K27me3+). The total number of DMRs is indicated on each bar.

cells, raising questions about the limits of plasticity between differentially polarized monocytes, and whether the induced epigenetic changes can be reversed. To study the DNA methylation dynamics associated with the GM-/M-CSF axis and to see whether the methylation changes are reversible, we differentiated monocytes with GM-CSF or M-CSF for 7 days and then swapped the cytokines to redifferentiate for a further 7 days (Figure 4).We used this method to analyze DNA methylation levels in seven genes differentially methylated between Mø-GM and Mø-M. Two of these (*STAB1* and *IL1RN*) did not respond to the cytokine switch and all the other analyzed genes underwent demethylation after exposure to GM-CSF or M-CSF, regardless of their previous polarization status. There was no reversion of DNA methylation changes after the cytokine switch, only the addition of new demethylation events. These methylation changes were not due to the extended cultivation period, since Mø-GM-specific genes did not respond to M-CSF even after 14 days exposure to this cytokine (Figure S2). Similarly, Mø-M-specific genes did not change their methylation status after a differentiation period of 14 days with GM-CSF, indicating that the annotated changes were specifically linked to the stimuli. Overall, these results suggest that the resulting cells were not completely repolarized at the epigenetic level after the cytokine switch, since they retained the DNA methylation changes induced by each cytokine. However, we also wanted to establish whether the exchange of the cytokines was associated with functional changes or, conversely, if the polarized cells were completely locked into a specific phenotype after their initial stimulation. First, we analyzed the phagocytic potential of these cells by measuring their ability to incorporate fluorescent-labeled zymosan. Although we observed that Mø-M cells captured zymosan more efficiently (68.5% labeled cells) than Mø-GM (42%), the phagocytic potential decreased after the extended cultivation period (40%) and non-significant differences were observed between groups (Figure S3A). On the other hand, the cytokine profile (IL6, IL19, CXCL1, CXCL5, and CXCL6) in cell supernatants showed a moderate response to GM-CSF in Mø-M cells, implying that they retain some plasticity (Figure S3B). We also tested two cytokines associated with Mø-M polarization: IL10 and CCL2. IL10 was undetected but we confirmed that CCL2 was produced in large quantities in response to M-CSF. However, the

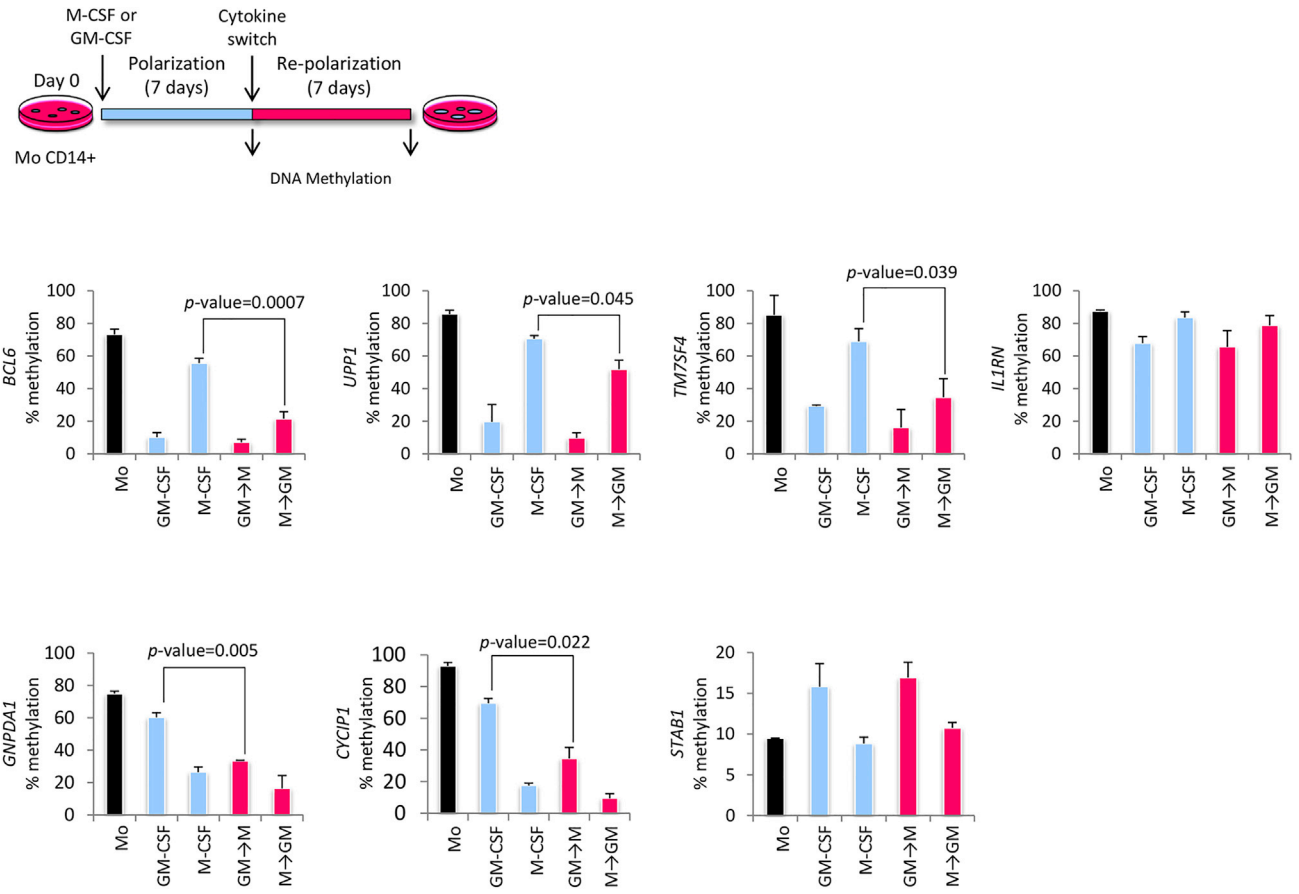

Figure 4. DNA Methylation Analysis of Mø-GM and Mø-M Cells after *In Vitro* Cytokine Switching

Human monocytes were first polarized *in vitro* for 7 days (long-term polarization) with M-CSF or GM-CSF. After this period, cytokines were exchanged and cells were allowed to differentiate for a further 7 days. DNA methylation levels were analyzed by pyrosequencing in three biological replicates. DNA methylation is represented as the average percentage of methylation of all CpG sites within the amplified region. Differences between groups were assessed with a Student's independent-samples t test (two tailed) (± SD).

addition of M-CSF did not significantly increase the production of CCL2 in Mø-GM cells.

Transcriptional Reprogramming and Chromatin Remodeling after Short-Term Polarization with GM-CSF and M-CSF

Epigenetic and transcriptomic analysis of long-term polarized monocytes could be the result of secondary signals associated with the induction of other transcription regulators or even be due to autocrine signaling throughout cytokine production. In order to study how the GM-/M-CSF signal is integrated at the chromatin level and reduce possible pleiotropic effects, we analyzed chromatin accessibility (ATAC-seq) and mRNA transcription after only 12 h exposure to M-CSF or GM-CSF (hereafter referred to as short-term polarization). By this method, RNA sequencing (RNA-seq) profiles showed that GM-CSF exposure induced a much more extensive transcriptional shift than M-CSF (Figure 5A; Table S5). M-CSF-exposed cells showed a phenotype intermediate between monocytes and GM-CSF-exposed cells since 52% (533) of the M-CSF genes are also induced by GM-CSF (Figure 5B). At the epigenetic level, we annotated 3,219 newly created regions of accessible chromatin (ATAC peaks) around the TSS, in contrast with M-CSF-treated monocytes in which only 10 genes were annotated (Table S6). Moreover, among the 1,206 genes upregulated in response to GM-CSF, 298 (24%) acquired at least one peak around the TSS, including many inflammatory and immune-related genes such as *IL1B*, *CD1C*, *CXCL1*, *CXCL5*, and *CISH*. In general, quantitative analysis of the ATAC-seq signal across the whole length of the gene indicated that genes overexpressed in response to both cytokines showed overall greater chromatin accessibility levels than the average values in other gene regions (Figure 5C). In response to GM-CSF, overexpressed genes showed greater chromatin accessibility ($p = 0.005$). This association was not observed as clearly with M-CSF ($p = 0.22$) (Figure 5C).

We also wanted to evaluate how chromatin accessibility was associated with histone occupancy. The increase of ATAC-seq signaling in response to GM-CSF and M-CSF clearly overlapped previously annotated regions in GM-CSF-activated monocytes (Schmidt et al., 2016), including accessible promoters (H3K4me3+/H3K27Ac+), poised promoters (H3K4me3+/H3K27me3+), strong enhancers (H3K27Ac+/H3K4me1+), and

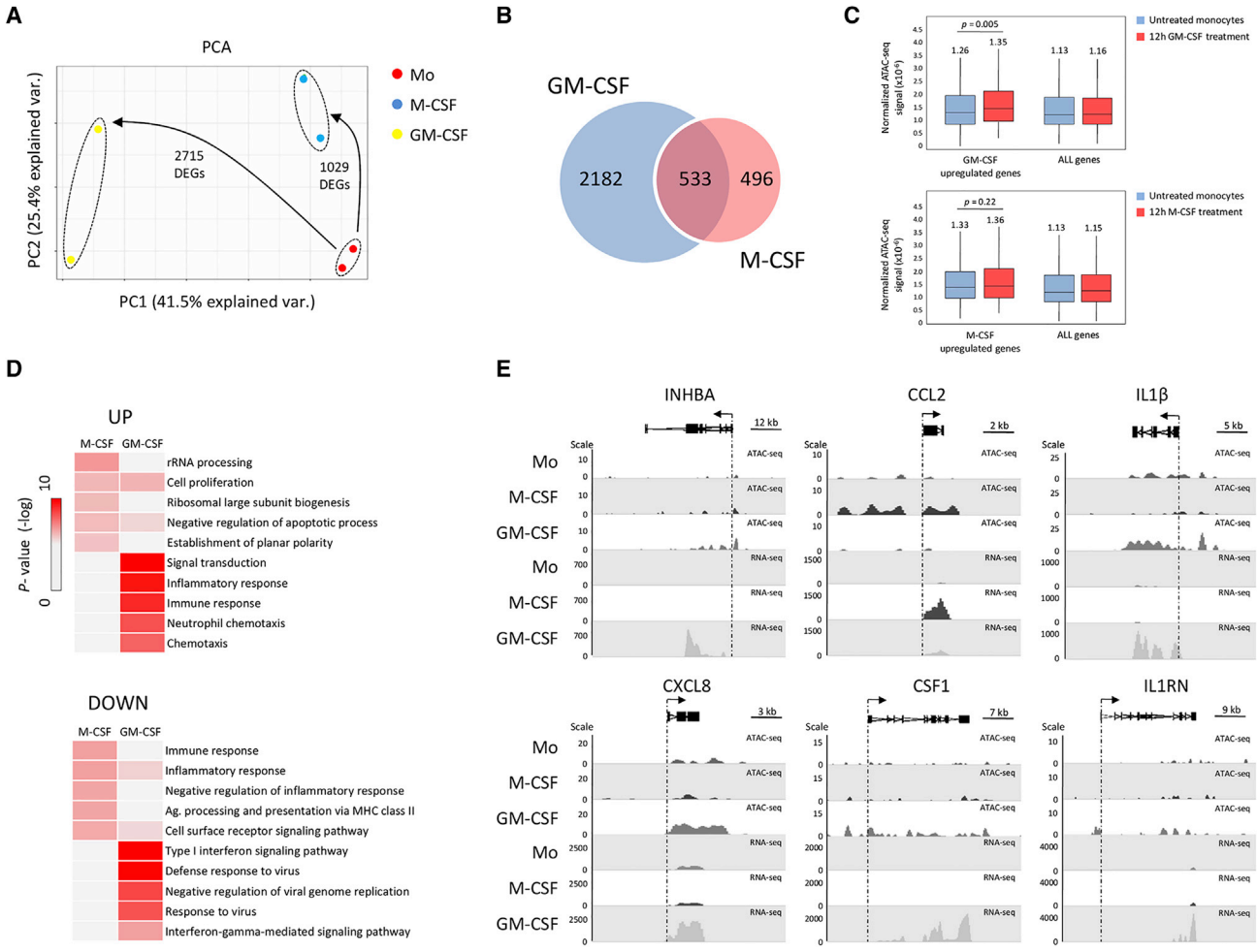

Figure 5. Transcriptional and Epigenetic Reprogramming during Short-Term Polarization

(A) Principal component analysis of RNA-seq data after 12 h exposure with M-CSF or GM-CSF in two biological replicates.

(B) Venn diagram showing the number of genes differentially expressed between untreated monocytes and monocytes exposed for 12 h with M-CSF and GM-CSF.

(C) Quantitative analysis of normalized ATAC-seq signal in genes upregulated in response to GM-CSF or M-CSF. Whiskers represent 1.5 * interquartile range. Differences between groups were assessed with a Mann–Whitney U test.

(D) Gene Ontology analysis of differentially expressed genes in response to both cytokines (12 h). Only the 10 top-ranked GO categories among upregulated and downregulated genes are represented.

(E) Transcription and chromatin accessibility of representative genes. TSS is indicated by an arrow. RNA-seq and ATAC-seq signals are represented across the entire length of the gene.

poised enhancers (H3K4me1+/H3K27me3+) (Figure S4A). Nonetheless, chromatin accessibility was greater in strong enhancers when activated with GM-CSF than with M-CSF.

Gene ontology analysis showed that short-term polarization induced upregulation of inflammatory and immune response genes by GM-CSF, but induced downregulation after M-CSF exposure (Figure 5D), arguing in favor of an opposing action. As previously indicated, however, approximately 50% of M-CSF-altered genes were also included in the GM-CSF program, and included the upregulation of angiogenesis (*WNT5A*, *SERPINE1*, *ADM2*, etc.) and cell adhesion pathways (*LIMA1*, *FERMT2*, *CTTN*, *CD93*, *SMAGP*, etc.) and downregulation of inflammation-related genes (*LY75*, *LYZ*, *TNFRSF8*, *TLR5*, *SERPINF1*, *CCR2*, etc.) (Table S5). In any case, these transcriptional dynamics were frequently associated with nucleosome remodeling, including many genes associated with the inflammatory and immune response, such as *IL1B*, *CXCL8*, *CXCL5*, *ALOX5AP*, and *IL1RN*, in which transcriptional overexpression was associated with a gain of chromatin accessibility (Figure 5E). Importantly, among the genes most overexpressed after GM-CSF treatment were M-CSF, encoded by the *CSF1* gene (552-fold change), and the activin A, which is encoded by *INHBA* (789-fold change), indicating that cytokine production occurs very rapidly after activation.

Dissection of the GM-CSF-Mediated Signal Transduction in Human Monocytes

Understanding how the signals in the tissue microenvironment contribute to the activation of the inflammatory pathways in macrophages is critical to the development of efficient immunomodulatory therapies. The extensive transcriptomic and epigenetic remodeling associated with GM-CSF exposure prompted us to investigate in more detail how signal transduction mediated by the GM-CSF receptor contributes to the development of the inflammatory program. Canonical GM-CSF receptor signaling is dependent on the tyrosine kinase of jak 2 (JAK2), which triggers the activation of the STAT5, Ras/mitogen-activated protein kinase (MAPK) and PI-3 kinase (PI3K) pathways (Hercus et al., 2009). However, it is not clear how each of these modules is associated with inflammation or whether they act cooperatively or by a self-regulatory mechanism. In order to study the specific contribution of each signaling module, we pharmacologically inhibited GM-CSF receptor signaling mediated by JAK2 with ruxolitinib (commonly used for treating myeloproliferative disorders) and downstream at the MEK level with trametinib (used for melanoma treatment), and inhibited PI3K with wortmannin (Figure 6A). The effective inhibition of each drug was validated by western blot analysis of STAT5, AKT, and extracellular signal-regulated kinase 1/2 (ERK1/2) phosphorylation (Figure 6A). Our results indicated that, as expected, JAK2 inhibition with ruxolitinib prevented signaling in all downstream signaling modules, whereas trametinib only reduced ERK1/2 phosphorylation. Nonetheless, it is important to note that although PI3K inhibition produced total abrogation of AKT phosphorylation, it also moderately reduced the level of ERK phosphorylation, suggesting some crosstalk downstream of this pathway.

Analysis of chromatin accessibility showed that treatment with any of the inhibitors resulted in the almost complete abrogation of the GM-CSF-induced open chromatin regions around the TSS (Table S6). Similarly, the increase of chromatin accessibility associated with GM-CSF activation in regulatory regions identified by histone occupancy was also profoundly disrupted when GM-CSF receptor signaling was blocked (Figure S4B), indicating that the signaling pathways downstream of this receptor are critical for chromatin remodeling. In addition, we scanned the newly created regions of accessible chromatin for transcription factor (TF) binding motifs. We found that the M-CSF response was associated with STAT binding motifs (STAT4, STAT5, and STAT6) and the zinc finger protein ZNF168 (Table S7). Likewise, the GM-CSF signature was much more clearly enriched with STAT5 binding motifs (552 regions with the binding motif). This result was expected because STAT5 is the canonical signaling module downstream of the GM-CSF receptor. In general, the GM-CSF response had a much richer TF binding profile that included BATF, JunC, and Atf3 among its highest-ranked factors. Interestingly, the GM-CSF signature was almost totally erased when GM-CSF signaling was inhibited, showing a TF binding profile similar to the M-CSF-treated monocytes.

On the other hand, the differential contribution of each signaling module was more clearly observed at the transcriptional level, as shown by principal component analysis (Figure 6B; Table S5). This showed that treatment with GM-CSF in the presence of the JAK2 inhibitor (iJAK) almost totally abrogated the transcriptional changes associated with this cytokine, whereas the MEK inhibitor (iMEK) had a much weaker effect. The latter result was expected, since only one signaling module was affected. A more surprising finding was that treatment with the inhibitor of PI3K (iPI3K) profoundly disrupted the GM-CSF signaling program. To explore the functional contribution of each signaling module, we performed gene clustering and ontology analysis with all the induced genes in each sample set with respect to untreated monocytes (Figure 6C). Clusters C2, C3, C4, and C5 included genes upregulated in monocytes after exposure to GM-CSF. These cluster profiles fade away in the presence of iJAK, indicating that they were mostly composed of JAK2-dependent genes. Among them, most inflammatory and immune response genes were identified in clusters C2 and C3, including the inflammatory interleukins (*IL1B*, *IL6*, *IL19*, etc.) and chemokines (*CXCL5* and *CXCL8*). These two clusters were also disrupted in the presence of iMEK but not by iPI3K, indicating that the inflammatory program induced by JAK2 was in part incorporated through the MAPK module. In some genes, such as *IL1B* and *CXCL5*, these transcriptional changes were accompanied by chromatin remodeling, and showed reduced accessibility in response to iJAK and iMEK, but not with iPI3K (Figure 6D). Clusters C4 and C5, on the other hand, corresponded to JAK2-dependent genes whose expression was mediated by the PI3K module and that included many genes associated with intracellular signaling (*PPARG*, *RTKN*, *NDRG2*, etc.), cytoskeleton (LIMK1 and ANK1), and immune function (*CCL24*, *IL36B*, *CD1A*, etc.), although inflammatory genes were mostly absent (Figure 6C). The *CSF1* gene (encoding M-CSF) was also included in cluster C5, indicating that M-CSF production was mediated by the PI3K module (Figure 6D). In contrast, the C6 cluster comprises a large subset of genes that were only upregulated in cells treated with GM-CSF in the presence of iPI3K. Interestingly, gene ontology analysis of this cluster showed substantial enrichment of pro-inflammatory genes (> 60 genes) (*CCL20*, *CXCL1*, *CASP4*, *IL23A*, etc.), while only some, such as *IL10*, may be considered anti-inflammatory genes, indicating that inhibition of the PI3K module stimulated the inflammatory program. In addition, the cytokine profile in the cell supernatant confirmed that iJAK and iMEK impaired the release of many of the cytokines associated with the inflammatory response (IL6, IL19, CXCL1, CXCL6, and CXCL5) while iPI3K produced the opposite effect, corroborating the pro-inflammatory role of the PI3K pathway in stimulated monocytes (Figure S5A). Conversely, M-CSF had very different dynamics, being the only cytokine that was more strongly inhibited by iPI3K than by iMEK.

Finally, since M-CSF expression was also regulated by PI3K, we examined whether the pro-inflammatory effect associated with iPI3K could be mediated by the inhibition of M-CSF production. With this aim, we blocked the M-CSF signal after GM-CSF stimulation to see whether this enhanced the expression of inflammatory genes to a similar degree as PI3K inhibition. Neither inhibiting M-CSF with a neutralizing antibody nor inhibiting the c-fms tyrosine kinase activity of the M-CSF receptor produced a significant increase in *IL1B* or *IL6* expression levels, suggesting that the overexpression of these genes was mediated by other mechanisms (Figure S5B).

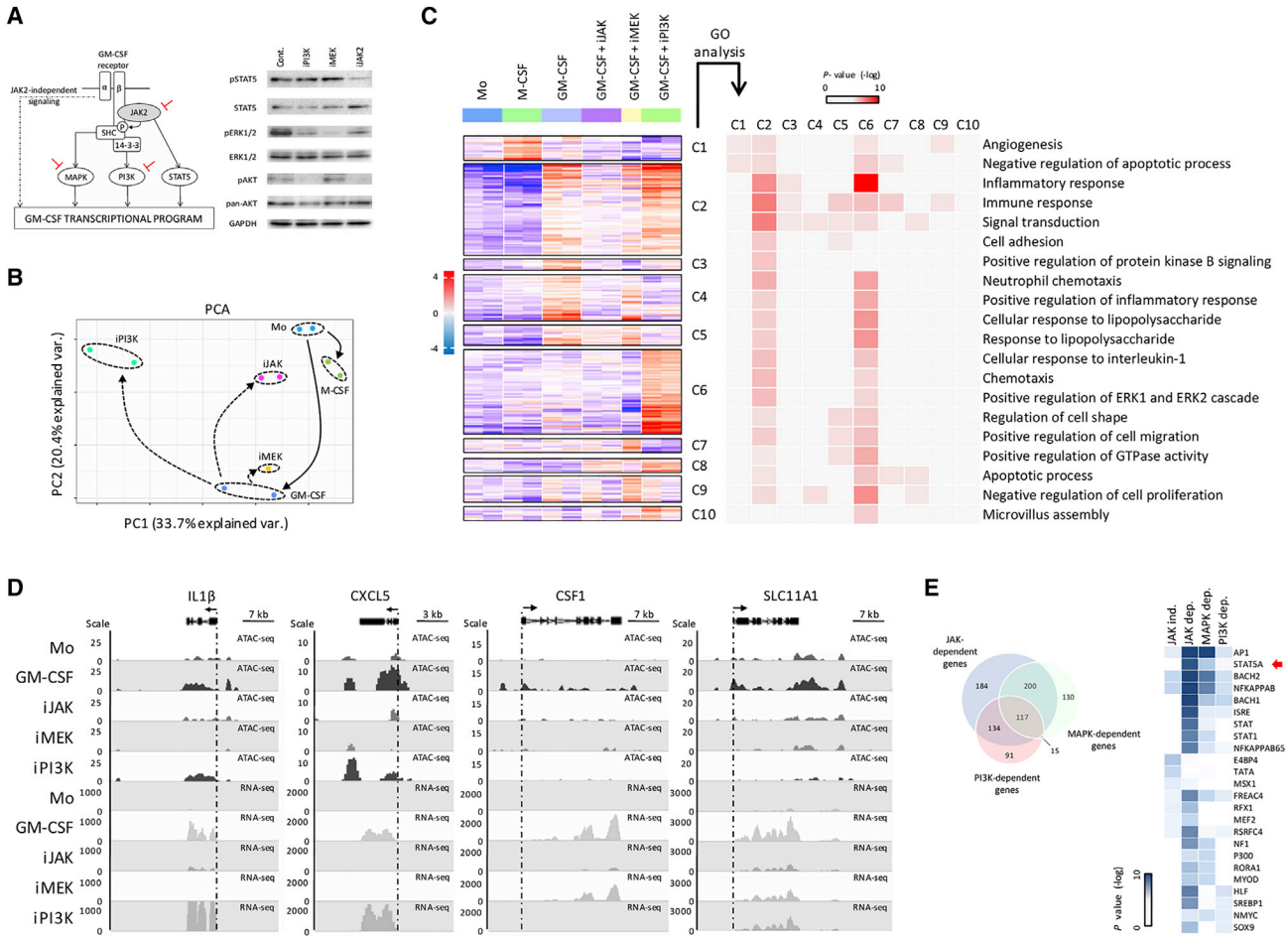

Figure 6. Dissection of GM-CSF-Mediated Signaling Modules in Human Monocytes

(A) Simplified representation of the main signaling modules mediated by GM-CSF receptor and western blot analysis of GM-CSF signaling after 30 min of stimulation in human monocytes. Activation of the PI3K signaling pathway was studied at the AKT level, and ERK1/2 phosphorylation was used to confirm inhibition of MEK activity. AKT (pan-AKT) and phospho-AKT (pAKT) correspond to the same samples probed in a different blot.

(B) Principal component analysis of RNA-seq profiles in GM-CSF-stimulated monocytes in the presence of iJAK, iMEK, or iPI3K (two biological replicates).

(C) Unsupervised gene cluster heatmap of induced genes (FC > 2) in Mo after stimulation with M-CSF and GM-CSF, or with the inhibitors of the JAK, MEK, and PI3K pathways. Gene ontology analysis of each cluster is shown in the right panel.

(D) Transcription and chromatin accessibility of representative genes.

(E) Venn diagram showing the number of GM-CSF-upregulated genes that are dependent on the JAK2, MAPK, or PI3K pathways. The transcription factor binding profile of each gene subset is shown in the right panel.

Our pharmacological strategy enabled us to identify GM-CSF-induced genes (upregulated or repressed, fold change [FC] > 2, adjusted value of $p < 0.05$) that were JAK2 dependent and, downstream, MAPK or PI3K dependent (a complete list of genes is provided in Table S8). In this way, we identified 1,348 JAK2-dependent and 1,368 JAK2-independent genes. In general, we observed that the inflammatory program seemed to be preferentially regulated through JAK2, although the JAK2-independent gene subset was significantly enriched in chemokines (*CXCL1*, *CXCL2*, *CCL24*, etc.) and some interleukins such as *IL24* (Table S8). Among the genes upregulated downstream of JAK2, there were 462 MAPK-dependent and 357 PI3K-dependent genes, most of which, as expected, were also JAK2 dependent (Figure 6E). On the other hand, enrichment analysis of conserved TF binding sites among GM-CSF-upregulated genes had significantly different profiles. Upregulated JAK2-dependent genes were considerably more enriched in TF binding sites, including BACH1, STATs (especially STAT5A), and interferon-stimulated response elements (ISREs). These were mostly absent from the JAK2-independent gene subset. Conversely, MAPK-dependent genes showed a similar TF profile to JAK2-dependent genes, but nuclear factor κB (NF-κB) and AP1 were overrepresented in this subset (although also present in the other gene subsets), while PI3K-dependent genes were characterized by an absence of STAT binding sites. Overall, these results indicated that each signaling module is associated with a differential TF signature, albeit one with common elements, including BACH1, BACH2, and NF-κB.

DISCUSSION

Consistent with previous results (Lacey et al., 2012; Ushach and Zlotnik, 2016), our data show that transcription profiles between GM-CSF- and M-CSF-polarized monocytes give rise to opposing phenotypes in the context of the inflammatory program. However, it is not clear how monocytes integrate these signals *in vivo*, since both cytokines are commonly found in the inflammatory microenvironment (Hamilton, 2008). Our findings indicate that epigenetic rewiring induced by GM-CSF is much more extensive than by M-CSF, at least under our *in vitro* conditions. It is possible that different culture conditions could produce different results and that a higher M-CSF concentration might increase the degree of epigenetic remodeling during polarization. Nonetheless, it is significant that most epigenetic changes induced by M-CSF are also induced by GM-CSF, while M-CSF was unable to induce most of the GM-CSF-stimulated changes, especially those associated with inflammatory pathways. Thus, M-CSF-polarized monocytes emerged as being in a less differentiated state, closer to undifferentiated monocytes than to cells differentiated with GM-CSF. As a result, from a transcriptional and epigenetic perspective, the notion that both cytokines perform opposing actions is barely supported, at least with respect to non-inflammatory functions. This is further reinforced by the fact that none of the cytokines was able to reverse the epigenetic changes induced by the others, and an additive effect was all that was observed in the subset of genes analyzed after cytokine switching. Although a genome-wide DNA methylation analysis would have provided a more complete picture of the plasticity associated with the epigenetic landscape acquired during polarization, none of the analyzed genes showed reversion of these changes. Therefore, it seems that polarized monocytes maintain at least a partial epigenetic memory associated with the different stimuli to which they have been exposed, while retaining the potential to respond to new signals in the tissue microenvironment, as demonstrated by the cytokine production in Mø-M cells stimulated with GM-CSF. Interestingly, a previous report described that M2-polarized monocytes retained the ability to respond to pro-inflammatory stimuli (LPS and interferon γ [IFNγ]) while M1 cells were not capable of responding to IL4 (Van den Bossche et al., 2016). The authors demonstrated that this process was due to a mitochondrial dysfunction in M1 monocytes that prevents the acquisition of M2 metabolic traits. Therefore, these results suggest that the M1 phenotypes are less phenotypically plastic, as they would represent a terminal differentiation state, an interpretation that would be consistent with the greater epigenetic drift that we observed in monocytes polarized with GM-CSF.

The apparent duality between M-CSF and GM-CSF raises the critical question about how the two cytokines are coupled at the functional and molecular levels. To answer this, we investigated the transcriptional and epigenetic rewiring during short-term polarization, reducing pleiotropic effects associated with the *in vitro* differentiation process. Even within this experimental framework, transcriptional profiles clearly show that M-CSF monocytes have an intermediate phenotype closer to that of control monocytes, while GM-CSF monocytes are associated, yet again, with much more widespread transcriptional and epigenetic remodeling. Integration of the GM-CSF signal in the chromatin occurs rapidly and incorporates a significant fraction of the inflammatory program that is absent from M-CSF-stimulated monocytes. The mechanisms by which GM-CSF induces deeper epigenetic rewiring are not clear, although *in vitro*-differentiated monocytes are known to differentially express epigenetic enzymes, including DNA methyltransferases (DNMTs), in response to different stimuli (Kittan et al., 2013). Therefore, tight transcriptional regulation of these enzymes may be essential for epigenetic remodeling during polarization. Regardless of this, we did not observe any differential expression of any DNMT enzyme between M-CSF and GM-CSF stimulation. Further studies are needed to clarify this matter.

An important finding of our analysis is that GM-CSF stimulation is intrinsically associated with the overexpression of M-CSF, which is among the most highly upregulated genes (> 500-fold change), as well as other cytokines that can potentially initiate autocrine signaling, such as *activin A* (789-fold change) and *IL-19* (102-fold change). Indeed, transcriptional overexpression of *CSF1* (M-CSF) in response to GM-CSF has been reported before in transcriptomic studies (Lacey et al., 2012). Also, activin A production in response to GM-CSF has been documented, demonstrating that its expression is associated with M1 skewing by blocking the acquisition of M2 phenotypes (Sierra-Filardi et al., 2011). Consequently, stimulation with GM-CSF is associated with a downstream autocrine signaling cascade that fundamentally contributes to monocyte polarization. Regardless, M-CSF production in GM-CSF-exposed monocytes explains the overlap of the transcriptional and epigenetic programs induced by both cytokines.

The complex regulatory networks associated with GM-CSF encouraged us to examine the GM-CSF signaling mediated by its receptor in even greater detail, and we were able to demonstrate that a very significant fraction of the inflammatory program is directed through JAK2 and the downstream MAPK pathway. Since MAPK targeting is enough to prevent a significant fraction of the inflammatory program, it would be worth investigating whether therapies that attempt to block GM-CSF, which is a central mediator of inflammation and tissue destruction in autoimmune diseases such as rheumatoid arthritis (RA) (Shiomi et al., 2016), could be complemented by MAPK targeting. On the other hand, blockage of the PI3K module stimulates the expression of many genes associated with inflammation, suggesting that it could act as a negative regulator of the inflammatory program to prevent an exacerbated inflammatory response. This result is consistent with a previous *in vitro* study in which the PI3K-Akt pathway was associated with the negative regulation of Toll-like receptor (TLR) signaling (Luyendyk et al., 2008). *In vivo* studies have also revealed that inhibition of PI3K activity in septic mice results in very significant increases in serum levels of inflammatory cytokines (IL1-β, IL-2, IL-6, IL-10, IL-12, and TNF-α) (Williams et al., 2004). Specific PI3Kγ inhibition has been shown to convert TAMs into pro-inflammatory phenotypes (Kaneda et al., 2016), suggesting that PI3K acts as a compensatory mechanism that suppresses pro-inflammatory processes. It should be noted that PI3K inhibition also strongly induces *IL-10* expression, so the balance between pro- and anti-inflammatory functions is not yet clear. In addition, it should be mentioned that,

in our study, we did not specifically dissect the STAT5 pathway. Nonetheless, most JAK2-dependent genes that are not inhibited by iMEK or iPI3K (which include important genes such as *INHBA*, *CISH*, *IL19*, and *CCL22*) are probably STAT5 dependent, since this is one of the major singling pathways associated with the GM-CSF receptor.

It is important to highlight that, according to our data, *CSF1* (M-CSF) overexpression in response to GM-CSF is regulated by the PI3K pathway. Since our genomic data showed M-CSF signaling to be associated with downregulation of the inflammatory program, it was tempting to speculate that the negative regulation of inflammation associated with the PI3K module might be mediated by the induction of autocrine production of M-CSF after GM-CSF stimulation. Nonetheless, our preliminary data indicate that at least the overexpression of the pro-inflammatory cytokines IL-1β and IL-6 is not dependent on autocrine signaling mediated by M-CSF, and that this mechanism might be more complex. However, it is likely that the M-CSF may help fine-tune the inflammatory program, since previous *in vitro* competition experiments have shown that the balance between the two cytokines can influence the polarization process toward pro- or anti-inflammatory phenotypes (Brochériou et al., 2011). Relative levels of both cytokines have also proved to be critical for the *in vivo* differentiation of macrophages during infection with *Mycobacterium tuberculosis* (Higgins et al., 2008), and blockage of the M-CSF receptor was associated with a polarization shift toward M1 phenotypes in tumor-bearing mice (Van Overmeire et al., 2016). In this context, both cytokines compete at the cellular level and the autocrine production of M-CSF via PI3K may contribute to the balance between them, acting as a regulatory loop within the local microenvironment.

Overall, our study provides a comprehensive view of how human monocytes integrate M-CSF and GM-CSF signaling in order to generate stable gene expression patterns during polarization, and how the two cytokines are functionally related during the process. Since the GM/M-CSF axis is proving to be a promising target in cancer and autoimmune diseases, understanding such a relationship will be critical to the successful development of suitable therapeutic strategies for treating these diseases.

STAR★METHODS

Detailed methods are provided in the online version of this paper and include the following:

SUPPLEMENTAL INFORMATION

Supplemental Information can be found online at https://doi.org/10.1016/j.celrep.2019.09.035.

ACKNOWLEDGMENTS

This work was supported by grants from the Plan Nacional de I+D+I 2013–2016 ISCIII (Institute of Health Carlos III; PI16/01318, PI17/01244, PI17/0119, PI16/1900, and PI19/00184); the Gobierno del Principado de Asturias; the PCTI-Plan de Ciencia, Tecnología e Innovación 2013-2017 (grant IDI/2018/144); FEDER "Funding Program of the European Union"; the Red Española de Investigación Renal (REDinREN) (RD16/0009/0020, RD016/0009/002, and RD016/0009/001); the Agencia Estatal de Investigación (AEI) (ayuda Juan de la Cierva-Incorporación; IJCI-2017-33347 to R.M.R.); and the Instituto de Salud Carlos III (Contratos Sara Borrell; CD16/00033 to C.H.). CIC bioGUNE support was provided by the Basque Department of Industry, Tourism and Trade (Etortek and Elkartek programs), the Innovation Technology Department of Bizkaia County, the CIBERehd Network, and Spanish MINECO, the Severo Ochoa Excellence Accreditation (SEV-2016-0644). We would like to thank Dr. David Mosén-Ansorena for assistance with the Illumina microarray analysis and Antonio Lopez-Vazquez for help with the Luminex analysis.

AUTHOR CONTRIBUTIONS

R.M.R., B.S.-A., and C.L.-L. designed the research and analyzed the data. R.M.R. wrote the paper. J.L.L., A.M.A., J.J.L., M.J.A.-B., and A.M.A. analyzed data. R.M.R., M.G., A.B.R., P.D.B., C.H., C.M.-M., J.R.V.-C., A.P.-K., and A.L.C. did the research.

DECLARATION OF INTERESTS

The authors declare no competing financial interests.

Received: February 11, 2019
Revised: June 27, 2019
Accepted: September 11, 2019
Published: October 22, 2019

REFERENCES

Aras, S., and Zaidi, M.R. (2017). TAMeless traitors: macrophages in cancer progression and metastasis. Br. J. Cancer *117*, 1583–1591.

Biswas, S.K., and Mantovani, A. (2010). Macrophage plasticity and interaction with lymphocyte subsets: cancer as a paradigm. Nat. Immunol. *11*, 889–896.

Brochériou, I., Maouche, S., Durand, H., Braunersreuther, V., Le Naour, G., Gratchev, A., Koskas, F., Mach, F., Kzhyshkowska, J., and Ninio, E. (2011). Antagonistic regulation of macrophage phenotype by M-CSF and GM-CSF: implication in atherosclerosis. Atherosclerosis *214*, 316–324.

Buenrostro, J.D., Giresi, P.G., Zaba, L.C., Chang, H.Y., and Greenleaf, W.J. (2013). Transposition of native chromatin for fast and sensitive epigenomic profiling of open chromatin, DNA-binding proteins and nucleosome position. Nat. Methods *10*, 1213–1218.

Corces, M.R., Buenrostro, J.D., Wu, B., Greenside, P.G., Chan, S.M., Koenig, J.L., Snyder, M.P., Pritchard, J.K., Kundaje, A., Greenleaf, W.J., et al. (2016). Lineage-specific and single-cell chromatin accessibility charts human hematopoiesis and leukemia evolution. Nat. Genet. *48*, 1193–1203.

Dobin, A., Davis, C.A., Schlesinger, F., Drenkow, J., Zaleski, C., Jha, S., Batut, P., Chaisson, M., and Gingeras, T.R. (2013). STAR: ultrafast universal RNA-seq aligner. Bioinformatics *29*, 15–21.

Du, P., Kibbe, W.A., and Lin, S.M. (2008). lumi: a pipeline for processing Illumina microarray. Bioinformatics *24*, 1547–1548.

Feng, J., Liu, T., Qin, B., Zhang, Y., and Liu, X.S. (2012). Identifying ChIP-seq enrichment using MACS. Nat. Protoc. *7*, 1728–1740.

Funes, S.C., Rios, M., Escobar-Vera, J., and Kalergis, A.M. (2018). Implications of macrophage polarization in autoimmunity. Immunology *154*, 186–195.

Gentleman, R.C., Carey, V.J., Bates, D.M., Bolstad, B., Dettling, M., Dudoit, S., Ellis, B., Gautier, L., Ge, Y., Gentry, J., et al. (2004). Bioconductor: open software development for computational biology and bioinformatics. Genome Biol. *5*, R80.

Hamilton, J.A. (2008). Colony-stimulating factors in inflammation and autoimmunity. Nat. Rev. Immunol. *8*, 533–544.

Hamilton, J.A., Cook, A.D., and Tak, P.P. (2016). Anti-colony-stimulating factor therapies for inflammatory and autoimmune diseases. Nat. Rev. Drug Discov. *16*, 53–70.

Harrow, J., Frankish, A., Gonzalez, J.M., Tapanari, E., Diekhans, M., Kokocinski, F., Aken, B.L., Barrell, D., Zadissa, A., Searle, S., et al. (2012). GENCODE: the reference human genome annotation for The ENCODE Project. Genome Res. *22*, 1760–1774.

Heinz, S., Benner, C., Spann, N., Bertolino, E., Lin, Y.C., Laslo, P., Cheng, J.X., Murre, C., Singh, H., and Glass, C.K. (2010). Simple combinations of lineage-determining transcription factors prime cis-regulatory elements required for macrophage and B cell identities. Mol. Cell *38*, 576–589.

Hercus, T.R., Thomas, D., Guthridge, M.A., Ekert, P.G., King-Scott, J., Parker, M.W., and Lopez, A.F. (2009). The granulocyte-macrophage colony-stimulating factor receptor: linking its structure to cell signaling and its role in disease. Blood *114*, 1289–1298.

Higgins, D.M., Sanchez-Campillo, J., Rosas-Taraco, A.G., Higgins, J.R., Lee, E.J., Orme, I.M., and Gonzalez-Juarrero, M. (2008). Relative levels of M-CSF and GM-CSF influence the specific generation of macrophage populations during infection with Mycobacterium tuberculosis. J. Immunol. *180*, 4892–4900.

Italiani, P., and Boraschi, D. (2014). From monocytes to M1/M2 macrophages: Phenotypical vs. functional differentiation. Front. Immunol. *5*, 514.

Kaneda, M.M., Messer, K.S., Ralainirina, N., Li, H., Leem, C.J., Gorjestani, S., Woo, G., Nguyen, A.V., Figueiredo, C.C., Foubert, P., et al. (2016). PI3Kγ is a molecular switch that controls immune suppression. Nature *539*, 437–442.

Kittan, N.A., Allen, R.M., Dhaliwal, A., Cavassani, K.A., Schaller, M., Gallagher, K.A., Carson, W.F., 4th, Mukherjee, S., Grembecka, J., Cierpicki, T., et al. (2013). Cytokine induced phenotypic and epigenetic signatures are key to establishing specific macrophage phenotypes. PLoS ONE *8*, e78045.

Kundaje, A., Meuleman, W., Ernst, J., Bilenky, M., Yen, A., Heravi-Moussavi, A., Kheradpour, P., Zhang, Z., Wang, J., Ziller, M.J., et al.; Roadmap Epigenomics Consortium (2015). Integrative analysis of 111 reference human epigenomes. Nature *518*, 317–330.

Lacey, D.C., Achuthan, A., Fleetwood, A.J., Dinh, H., Roiniotis, J., Scholz, G.M., Chang, M.W., Beckman, S.K., Cook, A.D., and Hamilton, J.A. (2012). Defining GM-CSF- and macrophage-CSF-dependent macrophage responses by in vitro models. J. Immunol. *188*, 5752–5765.

Langmead, B., and Salzberg, S.L. (2012). Fast gapped-read alignment with Bowtie 2. Nat. Methods *9*, 357–359.

Lawrence, T., and Natoli, G. (2011). Transcriptional regulation of macrophage polarization: enabling diversity with identity. Nat. Rev. Immunol. *11*, 750–761.

Lee, S.T., Xiao, Y., Muench, M.O., Xiao, J., Fomin, M.E., Wiencke, J.K., Zheng, S., Dou, X., de Smith, A., Chokkalingam, A., et al. (2012). A global DNA methylation and gene expression analysis of early human B-cell development reveals a demethylation signature and transcription factor network. Nucleic Acids Res. *40*, 11339–11351.

Li, B., and Dewey, C.N. (2011). RSEM: accurate transcript quantification from RNA-Seq data with or without a reference genome. BMC Bioinformatics *12*, 323.

Li, H., Handsaker, B., Wysoker, A., Fennell, T., Ruan, J., Homer, N., Marth, G., Abecasis, G., and Durbin, R.; 1000 Genome Project Data Processing Subgroup (2009). The Sequence Alignment/Map format and SAMtools. Bioinformatics *25*, 2078–2079.

Luyendyk, J.P., Schabbauer, G.A., Tencati, M., Holscher, T., Pawlinski, R., and Mackman, N. (2008). Genetic analysis of the role of the PI3K-Akt pathway in lipopolysaccharide-induced cytokine and tissue factor gene expression in monocytes/macrophages. J. Immunol. *180*, 4218–4226.

Martinez, F.O., and Gordon, S. (2014). The M1 and M2 paradigm of macrophage activation: time for reassessment. F1000Prime Rep. *6*, 13.

Neubert, N.J., Schmittnaegel, M., Bordry, N., Nassiri, S., Wald, N., Martignier, C., Tillé, L., Homicsko, K., Damsky, W., Maby-El Hajjami, H., et al. (2018). T cell-induced CSF1 promotes melanoma resistance to PD1 blockade. Sci. Transl. Med. *10*, eaan3311.

Park, S.H., Kang, K., Giannopoulou, E., Qiao, Y., Kang, K., Kim, G., Park-Min, K.H., and Ivashkiv, L.B. (2017). Type I interferons and the cytokine TNF cooperatively reprogram the macrophage epigenome to promote inflammatory activation. Nat. Immunol. *18*, 1104–1116.

Ramirez, R.N., El-Ali, N.C., Mager, M.A., Wyman, D., Conesa, A., and Mortazavi, A. (2017). Dynamic gene regulatory networks of human myeloid differentiation. Cell Syst. *4*, 416–429.e3.

Ries, C.H., Cannarile, M.A., Hoves, S., Benz, J., Wartha, K., Runza, V., Rey-Giraud, F., Pradel, L.P., Feuerhake, F., Klaman, I., et al. (2014). Targeting tumor-associated macrophages with anti-CSF-1R antibody reveals a strategy for cancer therapy. Cancer Cell *25*, 846–859.

Ritchie, M.E., Phipson, B., Wu, D., Hu, Y., Law, C.W., Shi, W., and Smyth, G.K. (2015). limma powers differential expression analyses for RNA-sequencing and microarray studies. Nucleic Acids Res. *43*, e47.

Rodriguez, R.M., Suarez-Alvarez, B., Mosén-Ansorena, D., García-Peydró, M., Fuentes, P., García-León, M.J., Gonzalez-Lahera, A., Macias-Camara, N., Toribio, M.L., Aransay, A.M., and Lopez-Larrea, C. (2015). Regulation of the transcriptional program by DNA methylation during human αβ T-cell development. Nucleic Acids Res. *43*, 760–774.

Ross-Innes, C.S., Stark, R., Teschendorff, A.E., Holmes, K.A., Ali, H.R., Dunning, M.J., Brown, G.D., Gojis, O., Ellis, I.O., Green, A.R., et al. (2012). Differential oestrogen receptor binding is associated with clinical outcome in breast cancer. Nature *481*, 389–393.

Saeed, S., Quintin, J., Kerstens, H.H., Rao, N.A., Aghajanirefah, A., Matarese, F., Cheng, S.C., Ratter, J., Berentsen, K., van der Ent, M.A., et al. (2014). Epigenetic programming of monocyte-to-macrophage differentiation and trained innate immunity. Science *345*, 1251086.

Sander, J., Schmidt, S.V., Cirovic, B., McGovern, N., Papantonopoulou, O., Hardt, A.L., Aschenbrenner, A.C., Kreer, C., Quast, T., Xu, A.M., et al. (2017). Cellular differentiation of human monocytes is regulated by time-dependent interleukin-4 signaling and the transcriptional regulator NCOR2. Immunity *47*, 1051–1066.e12.

Schmidt, S.V., Krebs, W., Ulas, T., Xue, J., Baßler, K., Günther, P., Hardt, A.L., Schultze, H., Sander, J., Klee, K., et al. (2016). The transcriptional regulator network of human inflammatory macrophages is defined by open chromatin. Cell Res. *26*, 151–170.

Shannon, P., Markiel, A., Ozier, O., Baliga, N.S., Wang, J.T., Ramage, D., Amin, N., Schwikowski, B., and Ideker, T. (2003). Cytoscape: a software environment for integrated models of biomolecular interaction networks. Genome Res. *13*, 2498–2504.

Shiomi, A., Usui, T., and Mimori, T. (2016). GM-CSF as a therapeutic target in autoimmune diseases. Inflamm. Regen. *36*, 8.

Sica, A., and Mantovani, A. (2012). Macrophage plasticity and polarization: in vivo veritas. J. Clin. Invest. *122*, 787–795.

Sierra-Filardi, E., Puig-Kröger, A., Blanco, F.J., Nieto, C., Bragado, R., Palomero, M.I., Bernabéu, C., Vega, M.A., and Corbí, A.L. (2011). Activin A skews macrophage polarization by promoting a proinflammatory phenotype and inhibiting the acquisition of anti-inflammatory macrophage markers. Blood *117*, 5092–5101.

Szklarczyk, D., Franceschini, A., Wyder, S., Forslund, K., Heller, D., Huerta-Cepas, J., Simonovic, M., Roth, A., Santos, A., Tsafou, K.P., et al. (2015). STRING v10: protein-protein interaction networks, integrated over the tree of life. Nucleic Acids Res. *43*, D447–D452.

Ushach, I., and Zlotnik, A. (2016). Biological role of granulocyte macrophage colony-stimulating factor (GM-CSF) and macrophage colony-stimulating factor (M-CSF) on cells of the myeloid lineage. J. Leukoc. Biol. *100*, 481–489.

Van den Bossche, J., Baardman, J., Otto, N.A., van der Velden, S., Neele, A.E., van den Berg, S.M., Luque-Martin, R., Chen, H.J., Boshuizen, M.C., Ahmed, M., et al. (2016). Mitochondrial dysfunction prevents repolarization of inflammatory macrophages. Cell Rep. *17*, 684–696.

Van Overmeire, E., Stijlemans, B., Heymann, F., Keirsse, J., Morias, Y., Elkrim, Y., Brys, L., Abels, C., Lahmar, Q., Ergen, C., et al. (2016). M-CSF and GM-CSF receptor signaling differentially regulate monocyte maturation and macrophage polarization in the tumor microenvironment. Cancer Res. *76*, 35–42.

Verreck, F.A., de Boer, T., Langenberg, D.M., Hoeve, M.A., Kramer, M., Vaisberg, E., Kastelein, R., Kolk, A., de Waal-Malefyt, R., and Ottenhoff, T.H. (2004). Human IL-23-producing type 1 macrophages promote but IL-10-producing type 2 macrophages subvert immunity to (myco)bacteria. Proc. Natl. Acad. Sci. USA *101*, 4560–4565.

Williams, D.L., Li, C., Ha, T., Ozment-Skelton, T., Kalbfleisch, J.H., Preiszner, J., Brooks, L., Breuel, K., and Schweitzer, J.B. (2004). Modulation of the phosphoinositide 3-kinase pathway alters innate resistance to polymicrobial sepsis. J. Immunol. *172*, 449–456.

Wynn, T.A., Chawla, A., and Pollard, J.W. (2013). Macrophage biology in development, homeostasis and disease. Nature *496*, 445–455.

Zhu, L.J., Gazin, C., Lawson, N.D., Pagès, H., Lin, S.M., Lapointe, D.S., and Green, M.R. (2010). ChIPpeakAnno: a Bioconductor package to annotate ChIP-seq and ChIP-chip data. BMC Bioinformatics *11*, 237.

STAR★METHODS

KEY RESOURCES TABLE

REAGENT or RESOURCE	SOURCE	IDENTIFIER
Antibodies		
STAT5	Cell Signaling Technology	Cat# 25656; RRID: AB_2798908
phospho-STAT5 (Tyr694)	Cell Signaling Technology	Cat# 4322; RRID: AB_10544692
p44/42 MAPK (Erk1/2) (137F5) Rabbit mAb	Cell Signaling Technology	Cat# 4695; RRID: AB_390779
Phospho-p44/42 MAPK (Erk1/2) (Thr202/Tyr204) (D13.14.4E) XP® Rabbit mAb	Cell Signaling Technology	Cat# 4370; RRID: AB_2315112
Akt (pan) (C67E7) Rabbit mAb	Cell Signaling Technology	Cat# 4691; RRID: AB_915783
Phospho-Akt (Thr308) (D25E6) XP Rabbit mAb	Cell Signaling Technology	Cat# 13038; RRID: AB_2629447
GAPDH (D16H11) XP® Rabbit mAb	Cell Signaling Technology	Cat# 5174; RRID: AB_10622025
M-CSF (Clone 26730)	R&D Systems	Cat# MAB216-SP; RRID: AB_2085064
Biological Samples		
Peripheral blood samples	Asturias Transfusion Centre, Spain	N/A
Chemicals, Peptides, and Recombinant Proteins		
Recombinant human GM-CSF	PeproTech	Cat#300-03
Recombinant human M-CSF	PeproTech	Cat#300-25
Wortmannin	Selleck Chemicals	Cat#S2758
Trametinib (GSK1120212)	Selleck Chemicals	Cat#S2673
Ruxolitinib (INCB018424)	Selleck Chemicals	Cat#S1378
KI20227	Tocris	Cat#4481/10
Cytochalasin D, actin polymerization inhibitor	Abcam	Cat#ab143484
Critical Commercial Assays		
EZ DNA methylation kit	Zymo Research	Cat#D5001
PyroMark kit	QIAGEN	Cat#978703
RNAqueous-Micro kit	Ambion	Cat#AM1931
SuperScript II Reverse Transcriptase Kit	Thermo Fisher Scientific	Cat# 18064014
TruSeq Stranded mRNA Library Prep	Illumina Inc.	Cat#20020594
Phagocytosis Assay Kit (Green Zymosan)	Abcam	Cat#ab234053
HumanMethylation450KBeadChip Kit	Illumina Inc.	Cat#WG-314-1003
HumanHT-12 v4 Expression BeadChip Kit	Illumina Inc.	Cat#BD-103-0204
TargetAmp Nano-g Biotin-aRNA Labeling Kit	Epicenter	Cat#TAN07924
Nextera DNA Library Preparation Kit	Illumina Inc.	Cat#FC-121-1030
CFSE	BioLegend	Cat#423801
Premix Ex Taq master mix	Takara	Cat#RR003A
TB Green Premix Ex TaqII	Takara	Cat#RR820A
CD14 MicroBeads, human	Miltenyi Biotech	Cat#130-050-201
Agencourt AMPure XP beads	Beckman Coulter	Cat#A63881
Luminex Human Magnetic Assay (9-Plex)	R&D Systems	Cat#LXSAHM-09
Deposited Data		
Raw microarray data	This paper	GEO: GSE123271
Raw RNA-seq and ATAC-seq data	This paper	GEO: GSE123574
Oligonucleotides		
Primer for qPCR: human TPT1, sense primer: 5′-GCAAGAACTGCAACAACAGC-3′	This paper	N/A
Primer for qPCR: human TPT1, reverse primer: 5′-GCTGATGAGGGGAGACAGAG-3′	This paper	N/A

(*Continued on next page*)

Continued

REAGENT or RESOURCE	SOURCE	IDENTIFIER
Primer for qPCR: human CSF1, sense primer: 5′-GATCGCGGACGGGTTGT-3′	This paper	N/A
Primer for qPCR: human CSF1, antisense primer: 5′-TTCAGCGGAGGCATTTCC-3′	This paper	N/A
Primer for pyrosequencing, see Table S1	This paper	N/A
Software and Algorithms		
Bioconductor project	Gentleman et al., 2004	https://www.bioconductor.org/
Lumi package	Du et al., 2008	https://www.bioconductor.org/
Cytoscape	Shannon et al., 2003	https://cytoscape.org/
Gephi	Gephi - The Open Graph Viz Platform	https://gephi.org/
FASTQC	Babraham Bioinformatics	https://www.bioinformatics.babraham.ac.uk/projects/fastqc/
bowtie2	Langmead and Salzberg, 2012	http://bowtie-bio.sourceforge.net/bowtie2/index.shtml
Picard	Broad Institute	http://broadinstitute.github.io/picard/
SAMtools view	Li et al., 2009	http://www.htslib.org/doc/samtools.html
MACS2	Feng et al., 2012	https://github.com/taoliu/MACS
Diffbind	Ross-Innes et al., 2012	https://www.bioconductor.org/
ChIPpeakAnno	Zhu et al., 2010	https://www.bioconductor.org/
SeqMonk	Babraham Bioinformatics	https://www.bioinformatics.babraham.ac.uk/projects/seqmonk/
STAR	Dobin et al., 2013	https://github.com/alexdobin/STAR
RSEM	Li and Dewey, 2011	https://github.com/deweylab/RSEM
GENCODE v26	Harrow et al., 2012	https://www.gencodegenes.org/
Homer (v4.10.4)	Heinz et al., 2010	http://homer.ucsd.edu/homer/

LEAD CONTACT AND MATERIALS AVAILABILITY

Further information and requests for resources and reagents should be directed to and will be fulfilled by the Lead Contact, Carlos Lopez-Larrea (inmuno@hca.es). This study did not generate new unique reagents.

EXPERIMENTAL MODEL AND SUBJECT DETAILS

Human Blood Samples

Peripheral Blood samples were obtained from healthy adult donors from the Asturias Transfusion Centre, Spain, after obtaining their written informed consent in accordance with the Declaration of Helsinki and the approved guidelines established by the Research Ethics Board of the Spanish Research Council. Information about donors' sex was not provided. Peripheral blood mononuclear cells (PBMCs) were isolated by density gradient centrifugation. CD14+ monocytes were isolated from PBMCs by magnetic bead separation using human CD14 MicroBeads (MiltenyiBiotec). Isolated cells were >95% pure, as shown by flow cytometry analysis.

METHOD DETAILS

Isolation of Human Monocytes, Ex Vivo Differentiation, and Treatment

For long-term polarization, monocytes were cultured in RPMI medium (Life Technologies) supplemented with 10% FCS (Thermo Fisher Scientific) and incubated with GM-CSF (1000 U/ml, PeproTech) or M-CSF (10 ng/ml, PeproTech) for 7 days. Cytokines were added to the medium every 2 days. For short-term polarization (12 h), cells were incubated with M-CSF or GM-CSF in the presence wortmannin (250 nM), trametinib (75 nM) or ruxolitinib (600 nM) (Selleck Chemicals). M-CSF signaling was inhibited with the c-fms tyrosine kinase inhibitor (KI20227, 100 nM) (Tocris) or with a neutralizing antibody against M-CSF (Clone 26730, 1 μg/ml) (R&D Systems).

Western Blotting

Cells were prepared by SDS lysis extraction in the presence of Pierce™ protease and phosphatase inhibitor (Thermo Fisher Scientific). After SDS-PAGE, proteins were detected by western blot analysis with antibodies against STAT5, phospho-STAT5 (Tyr694), ERK1/2, phosho-ERK1/2 (Thr202/Tyr204), phospho-AKT (Thr308), AKT (pan) and GAPDH (Cell Signaling Technology). Secondary antibodies conjugated with HRP were obtained from Thermo Fisher Scientific.

Cell Division Analysis

Cell division was analyzed with carboxyfluorescein succinimidyl ester (CFSE) staining at 1.25 μM (20 min, room temperature) (BioLegend). After incubation, CFSE was blocked for 10 minutes with 10% FCS (Thermo Fisher Scientific). Cell staining was analyzed in a Gallios Flow Cytometer (Beckman Coulter).

Phagocytosis Assay

In vitro phagocytosis was measured with FITC-labeled zymosan particles using a Phagocytosis Assay Kit (Green Zymosan) (Abcam). Briefly, cells under each condition were incubated for 1 h with 20 μM cytochalasin D (Abcam) as a negative control. Then, cells were incubated with FITC-zymosan particles for 3 h before analysis following the manufacturer's instructions. *In vitro* phagocytosis was quantified in a Gallios Flow Cytometer (Beckman Coulter).

Cytokine Detection and Measurement

Cell culture supernatants were collected and diluted 1:2 before analysis. Cytokine secretion was measured with a Luminex Human Magnetic Assay (9-Plex) (R&D Systems) following the manufacturer's protocol. This assay allowed the simultaneous detection of the following cytokines: IL1B, IL6, IL10, M-CSF, CXCL5, IL19, CXCL6, CXCL1 and CCL2. After cytokine labeling, protein concentration was measured in a Luminex 200™ system (Luminex Corporation).

Bisulfite Pyrosequencing

Sodium bisulfite modification of 500 ng of total DNA was performed with the EZ DNA methylation kit (Zymo Research) following the manufacturer's protocol. Modified DNA was amplified using the primers indicated in Table S9. After amplification, methylation levels were quantified with a PyroMark kit (QIAGEN) and the PyroMark Q24 system (Biotage), following the manufacturer's instructions.

Real-Time qRT-PCR

Total RNA was extracted using an RNAqueous-Micro kit (Ambion) and cDNA was synthesized from 1 μg of total RNA with a SuperScript II Reverse Transcriptase Kit (Thermo Fisher Scientific). Quantification was performed with TaqMan Gene Expression Assays (Applied Biosystems) for the *IL1B* (Hs01555410_m1) and *IL6* (Hs00174131_m1) genes using Premix Ex Taq master mix (Takara). Glyceraldehyde 3-phosphate dehydrogenase (*GAPDH*) (Hs02758991_g1) was used to normalize data, following the ΔΔCt method. Expression of *CSF1* was analyzed with TB Green Premix Ex TaqII (Tli RNase H Plus) (Takara) and the tumor protein translationally controlled 1 (*TPT1*) gene was used to normalize data. The 5′-GCAAGAACTGCAACAACAGC-3′ (sense) and 5′-GCTGATGAGGGGA GACAGAG-3′ (antisense) primers were used to amplify *CSF1*; 5′-GATCGCGGACGGGTTGT-3′ (sense) and 5′-TTCAGCGGAGG CATTTCC-3′ (antisense) were used to amplify *TPT1*.

DNA Extraction and Microarray Whole-Genome Methylation Profiling

Total DNA was extracted with a Genomic DNA Mini Kit (ATP Biotech), following the manufacturer's recommended protocol. DNA integrity was evaluated in TAE agarose gels. An EZ DNA methylation kit (Zymo Research) was used for sodium bisulfite conversion of 500 ng of total DNA. Whole-genome DNA methylation was analyzed with an Infinium HumanMethylation450KBeadChip Kit (Illumina Inc.), according to Illumina's Infinium HD assay methylation protocol. Datasets were generated from two biological replicates obtained from a pool of three individuals. Raw methylation data were decoded with GenomeStudio software (Illumina Inc.).

RNA Extraction and Microarray Whole-Genome Gene Expression Characterization

Total RNA was extracted using an RNAqueous-Micro kit (Ambion). RNA size and integrity were analyzed in RNA Nano Chips with a Bioanalyzer 2100 (Agilent), and genome expression was characterized with a HumanHT-12 v4 Expression BeadChip Kit (Illumina Inc.). Datasets were generated from three biological replicates obtained from a pool of three individuals. cRNA was synthesized with a TargetAmp Nano-g Biotin-aRNA Labeling Kit for the Illumina System (Epicenter). Amplification, labeling and hybridization were then performed according to Illumina's Whole-Genome Gene Expression Direct Hybridization Protocol. Raw expression data were obtained with GenomeStudio analytical software (Illumina Inc.).

Microarray Analysis

Raw data from GenomeStudio were analyzed using R packages from the Bioconductor project (Gentleman et al., 2004). Methylation data were background-corrected, $\log_2$-transformed, quantile-adjusted for color balance, and quantile-normalized with the lumi

package (Du et al., 2008). Gene expression data were background-corrected and $\log_2$-transformed. Probes with detection values of $p > 0.01$ were removed. To analyze DNA methylation, sex chromosomes were eliminated and site locations were recorded using Illumina's HumanMethylation450k annotations. Between-group pairwise methylation and expression comparisons were quantified. A linear model was fitted to the data and empirical Bayes-moderated t-statistics were calculated with the limma package. False discovery rates (FDRs) were adjusted using the Benjamini–Hochberg procedure. For gene expression data, only probes with an adjusted FDR $p < 0.05$ and >2-fold absolute value were analyzed. For DNA methylation we selected probes with an M-difference (ΔM) >1.5 and an adjusted FDR $p < 0.05$. Functional interaction network data were obtained from STRING v10 (Szklarczyk et al., 2015) and then built using Cytoscape software (Shannon et al., 2003). The resulting network was exported to Gephi, whereupon graphs were derived using the Fruchterman–Reingold clustering algorithm (https://gephi.org/). Gene ontology (GO) enrichment analysis was performed with the DAVID Web-based tool (https://david.ncifcrf.gov/).

Fast-ATAC and Sequencing

To analyze chromatin accessibility, we followed the Fast-ATAC protocol, which is specifically adapted for blood cells (Corces et al., 2016). Two biological replicates were used per condition. Briefly, 5,000 cells were resuspended in 50 μL of tagmentation mixture (25 μL TD buffer, 2.5 μL TDE1, 0.5 μL 1% digitonin and 22 μL water) (Nextera DNA Library Preparation Kit, Illumina Inc.) and incubated at 37°C for 30 minutes. After tagmentation, DNA was purified with MinElute PCR Purification kit and amplified as previously described (Buenrostro et al., 2013). A double-size selection using Agencourt AMPure XP beads was performed based on the ATAC-seq Protocol from Kaestner Lab (https://www.med.upenn.edu/kaestnerlab/protocols.html). Sequencing was carried out using a HiSeq 4000 platform (Illumina Inc.). Raw read data were converted into FASTQ format, and quality control was assessed using the FASTQC software (Babraham Bioinformatics). Adapters used for sequencing were removed with TrinGalore (Babraham Bioinformatics). Reads were aligned with bowtie2 (Langmead and Salzberg, 2012), mapping against the Human Genome 38 reference (hg38). The alignment was performed with the command "bowtie2 -X 2000–n 2," which supports paired-end read sequencing. Reads mapped to mitochondrial and unknown, random or sex chromosomes were removed. Duplicated reads were removed with Picard (http://broadinstitute.github.io/picard/) MarkDuplicates. Low-quality reads (MAPQ < 10) were removed using SAMtools view (Li et al., 2009). Results of the read mapping were exported as input for peak calling. In this step, peaks were called by MACS2 software (Feng et al., 2012) using the corresponding control group to call the peaks of the experimental group. MACS2 was run twice, once for single nucleosome detection with the following parameters (-g "hs" -p 0.01–nomodel–shift −37–extsize 73 –broad) and a second time for extended nucleosome detection (-g "hs" -p 0.01–nomodel–shift −100–extsize 200 –broad). Peaks of different experimental groups were compared using the Diffbind package (Ross-Innes et al., 2012), which yielded a set of differentially called peaks for each comparison. Those peaks were annotated and functionally characterized using the ChIPpeakAnno package (Zhu et al., 2010). To quantify the ATAC-seq signal along the entire length of the gene, we used a sliding window of 1,000 nucleotides to count the number of reads in each region. For each gene (hg38 genome), we took the region between the beginning and end of the gene and assigned an FPKM value to each gene. The FPKM values were calculated as (number of reads) / (1,000 × number of windows with signal in the gene × length window). We corrected sample bias with the Bland-Altman normalization by pairs, using the undifferentiated monocyte as the reference. This step was performed independently for each replicate. For visualization, ATAC signals were distributed in 200-bp windows, read counts where corrected to reads per million, and normalized according an averaged distribution of quantitated values across all datasets using SeqMonk tools (Babraham Bioinformatics). Motif enrichment was analyzed using HOMER (v4.10.4) (http://homer.ucsd.edu/homer/) (Heinz et al., 2010). Specifically, the "findMotifsGenome.pl" wrapper script was called to enable the use of the HOMER algorithm to evaluate the enrichment of known motifs. The input of this step is a list of genomic coordinates corresponding to the open chromatin regions detected by the ATAC seq experiment for each of the groups analyzed.

RNA Sequencing and Gene Expression Analysis

RNA was extracted from the same samples used for FAST-ATAC with an RNAqueous-Micro kit (Ambion). Integrity was analyzed in RNA Nano Chips with a Bioanalyzer (Agilent). Starting from 400 ng of total RNA, sequencing libraries were prepared following the "TruSeq Stranded mRNA Sample Preparation Guide (Part # 15031047 Rev. E)," with the corresponding kit (Illumina Inc. Cat.# RS-122-2101 and RS-122-2102, Set A and Set B, respectively). Sequencing was carried out using a HiSeq 2500 platform (Illumina Inc.). After trimming for adapters using trim_galore (Babraham Bioinformatics), reads were mapped using the STAR program (Dobin et al., 2013) against human genome (hg38), and the genes and transcripts were quantified with the RSEM program (Li and Dewey, 2011) using GENCODE v26 (Harrow et al., 2012). We used the TMM method and limma-voom transformation from rounded expected counts to normalize the non-biological variability (Ritchie et al., 2015). Differential expression between groups was evaluated using moderated t-statistics. Transcription factor enrichment of differentially expressed genes was analyzed by DAVID Web-based tool (UCSC_TFBS algorithm).

QUANTIFICATION AND STATISTICAL ANALYSIS

Statistical analyses were performed by Student's t test and Mann-Whitney U test using SPSS 16.0 software (IBM SPSS, Chicago, IL). The number of replicates are indicated in the legend of each figure. All data shown are the mean (±SD) of at least two biological replicates. Values of $p < 0.05$ were considered significant.

DATA AND CODE AVAILABILITY

Raw microarray data have been deposited in the NCBI Gene Expression Omnibus under accession number GEO: GSE123271. RNA-seq and ATAC-seq raw data were submitted to the NCBI Gene Expression Omnibus under accession number GEO: GSE123574.